
Article:
Comini, F., Palanca, M., Cristofolini, L. et al. (1 more author) (2019) Uncertainties of synchrotron microCT-based digital volume correlation bone strain measurements under simulated deformation. Journal of Biomechanics, 86. pp. 232-237. ISSN 0021-9290

https://doi.org/10.1016/j.jbiomech.2019.01.041

Uncertainties of Synchrotron microCT-based Digital Volume Correlation bone strain measurements under simulated deformation

F. Comini[a,b], M. Palanca [b], L. Cristofolini [b], E. Dall'Ara [a]*

[a] Department of Oncology and Metabolism and INSIGNEO Institute for in silico Medicine, University of Sheffield, UK
[b] Department of Industrial Engineering, School of Engineering and Architecture, Alma Mater Studiorum - Università di Bologna, Bologna, Italy

Corresponding Author.
Name Surname: Enrico Dall'Ara
Telephone number: +44 (0)114 2226175
E-mail: e.dallara@sheffield.ac.uk

Word count Abstract: 250

Word count Introduction-Discussion: 2345

Number of Figures: 5

Number of Tables: 1

ABSTRACT

Digital Volume Correlation (DVC) is used to measure internal displacements and strains in bone. Recent studies have shown that synchrotron radiation micro-computed tomography (SR-microCT) can improve the accuracy and precision of DVC. However, only zero-strain or virtually-moved test have been used to quantify the DVC uncertainties, leading to potential underestimation of the measurement errors.

In this study, for the first time, the uncertainties of a global DVC approach have been evaluated on repeated SR-microCT scans of bovine cortical bone (voxel size: 1.6μm), which were virtually deformed for different magnitudes and along different directions.

The results showed that systematic and random errors of the normal strain components along the deformation direction were higher than the errors along unstrained directions. The systematic percentage errors were smaller for larger virtual deformations. The random percentage error was in the order of 10% of the virtual deformation. However, higher errors were localized at the boundary of the volumes of interest, perpendicular to the deformation direction. When only the central region of the samples was considered (100 micrometers layers removed from the borders where the deformation was applied), the errors in the direction of virtual deformation were comparable to the errors in the unstrained directions.

In conclusion, the method presented to estimate the uncertainties of DVC is suitable for testing anisotropic specimens as cortical bone. The good agreement between the uncertainties in measurements of strain components obtained with this approach and with the simpler zero-strain-test suggests that the latter is adequate in the tested deformation scenarios.

KEYWORDS: Bone, Strain, Digital Volume Correlation, Synchrotron microCT, Uncertainties

1 INTRODUCTION

The Digital Volume Correlation (DVC) approach, introduced by Bay and colleagues in the 1999, can be used to measure displacement and strain inside heterogeneous materials as trabecular bone (Bay et al. 1999). Many applications of the DVC have been reported in the literature for bone tissues and biomaterials (Liu and Morgan, 2007; Madi *et al.*, 2013; Gillard *et al.*, 2014; Roberts *et al.*, 2014; Grassi and Isaksson, 2015; Zhu *et al.*, 2016; Tozzi *et al.*, 2017). Several studies have shown that the precision of the method decreases with increased DVC measurement spatial resolution (Dall'Ara *et al.*, 2014; Dall'Ara *et al.*, 2017). However, this is usually tested in zero-strain conditions by registering repeated scans of the same object, making difficult to evaluate the error of the method under loading, and the heterogeneous distribution of the uncertainties with respect to the direction of strain. Virtually deformed images have been used in the past to evaluate the accuracy and precision of Digital Image Correlation (Sun Y et al., 2005) or DVC (Hardisty MR et al., 2009). Nevertheless, in DVC applications, the measurement uncertainties assessed with virtually deformed images are underestimated, due to the fact that the typical noise observed in images acquired during time lapsed loading is not accounted for. Therefore, a realistic estimation of the measurement errors can be performed only by registering images acquired from repeated scans, one of which is virtually deformed. This approach has been used in this study.

DVC has been recently used also to evaluate the ability of finite element (FE) models in predicting the heterogeneous deformation in trabecular bone (Zauel 2005; Chen et al. 2017), in vertebral body (Jackman *et al.*, 2016*;* Costa et al. 2017) and in the mouse tibia (Oliviero *et al.,* 2018) scanned with micro-computed tomography (microCT). Nevertheless, the relatively low accuracy and precision in strain measurements at the single bone structural unit (10-50 micrometers), allowed to directly compare DVC measurements and FE models predictions for the displacement field or for strains only in large sub-regions of the specimen.

Two recent studies reported that high-resolution tomograms, based on Synchrotron radiation (SR-microCT), can improve the accuracy and precision of the DVC displacement and strain measurements (Christen et al. 2012; Palanca et al. 2017). With this approach, acceptable value of uncertainties in the strain measurements can be obtained with spatial resolution of approximately 40 μm, assessed with zero-strain tests (Palanca et al. 2017). Nevertheless, little is known about the DVC uncertainties when applied to a deformed specimen. Considering the complex structure of bone, a detailed analysis of the effect of the magnitude and direction of

deformation or distance from the border of the image on the outcomes of DVC algorithm is needed in order to better understand the potential of this technique.

The aim of this study was to quantify the strain measurement uncertainties of SR-microCT image-based DVC in cortical bone for different load magnitudes and along different loading directions. In particular, the results are compared to those obtained with simple zero-strain experiments in order to understand their applicability.

2 MATERIALS AND METHODS

2.1. Specimens preparation, SR-microCT scanning and image processing

The specimens used for the analyses were prepared and scanned in a previous study (Palanca et al. 2017). Briefly, four 3 mm in diameter and 12 mm in length cortical bone cylinders have been extracted from the diaphysis of a fresh bovine femur. Specimens were scanned at the Diamond-Manchester Imaging Beamline I13-2 of the Diamond Light Source, UK with a filtered (950 μm C, 2 mm Al, 20 μm Ni) polychromatic 'pink' beam (5–35 keV) of parallel geometry. Projections were acquired using a pco.edge 5.5 detector (PCO AG, Germany) coupled to a 750 μm-thick CdWO4 scintillator, with visual optics providing 4x total magnification and a field of view of 4.2x3.5 mm. Scanning parameters: 4001 projections, 180 degrees of continuous rotation, exposure time of 53 ms, and effective voxels size of 1.6 μm. Each specimen was scanned twice under zero-strain conditions (Scan1 and Scan2). Cubic volumes of interest (VOIs, side lengths 1000 voxels) were cropped from the middle of each reconstructed image.

Virtual deformations were applied using MeVisLab (MeVis Medical Solutions AG, Germany). Scan2 of each specimen has been axially compressed, applying a virtual affine deformation symmetric with respect to the center of the image, of 1%, 2% or 3% along X, Y or Z separately, for a total of 9 combinations. Trilinear interpolation was applied to the virtually deformed images. The image Z-axis was approximately aligned with the longitudinal axis of the diaphysis of the femur.

The images used in this study can be requested from the link: 10.15131/shef.data.7624958/10.15131/shef.data.7624958.

2.2. DVC protocol

In this study a global DVC protocol has been used to compute the strain field: BoneDVC (Dall'Ara *et al.*, 2014; Dall'Ara *et al.*, 2017). It is a combination of the elastic registration software Sheffield Image Registration Toolkit (ShIRT) (Barber and Hose, 2005; Barber et al. 2007) and a Finite Element (FE) software package (Mechanical APDL v. 14.0, Ansys, Inc., USA). A homogeneous cubic grid with a certain nodal spacing (NS) was superimposed to the two input images (Scan 1 and Scan 2) and the displacements at each node of the grid were computed by solving the registration equations. For all the DVC analyses, a nodal spacing of 25 voxels (40 μm) was used, which was found to be the best compromise between spatial resolution of the DVC and strain uncertainties in a previous zero-strain study (Palanca et al. 2017). The six components of strain at each node of the grid were computed by differentiating the displacement field by using the shape functions.

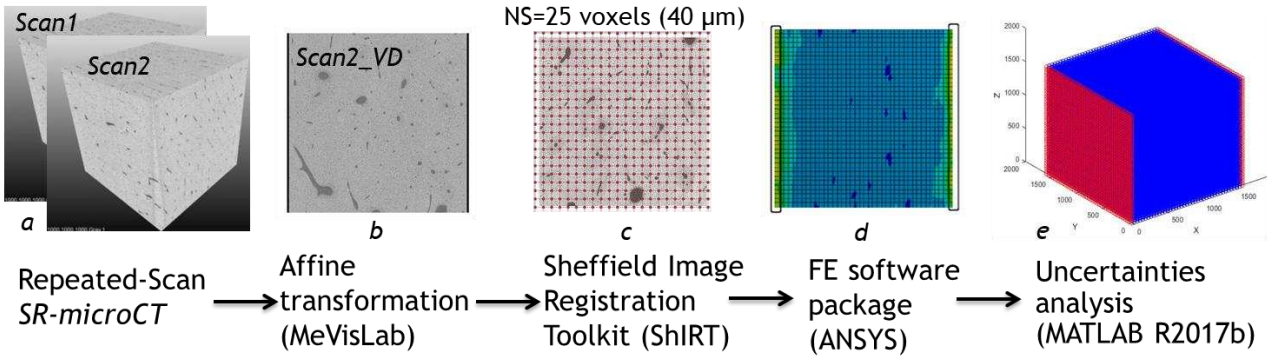

Figure 1*.Workflow used to investigate the precision and accuracy of the BoneDVC approach for measurement of strains in cortical bone loaded in compression. Two regions of interest are cropped from repeated Synchrotron microCT images of cortical bone specimens (Scan1 and Scan2, a). One of the repeated images is synthetically compressed along different directions using an affine transformation (b). A deformable registration is applied to the couple of undeformed (Scan1) and virtually deformed (Scan2_VD) images for a nodal spacing (NS) equal to 25 voxels, for each loading direction and load level (c). The registration grid is then converted to a finite element (FE) model and an FE software package is used to differentiate the displacement field into a strain field and to post-process the results (d). Finally, a custom-made script is used to compare the measured deformation with the nominal one (e).*

2.3. Uncertainties analysis

The strain measurement uncertainties were evaluated with a home-written script (MATLAB R2017b, The MathWorks, Inc.). The nodes outside the image (Figure 1b) have been excluded from the analysis.

The uncertainties of strain measurements were quantified with similar methods reported in the literature. The systematic and random errors were quantified for each component of strain (Gillard et al. 2014; Palanca et al.

2015) in order to evaluate any anisotropic behavior of the DVC uncertainties. Moreover, considering that in many cases the principal strains are used to define the failure behavior of bone, the minimum and maximum principal strains were also calculated. The mean absolute error (MAER) and the standard deviation of the error (SDER) were compute as average or standard deviation, among all nodes, of the average of the absolute difference between the values of the six components of strain calculated in each node and the nominal imposed strain value for that component (Liu and Morgan 2007; Palanca et al. 2016):

$$\text{MAER} = \frac{1}{N}\sum_{k=1}^{N}\left(\frac{1}{6}\sum_{c=1}^{6}\left|\varepsilon_{c,k} - \varepsilon_{\text{nom } c,k}\right|\right) \qquad \text{(Eq. 1)}$$

$$\text{SDER} = \sqrt{\frac{1}{N}\sum_{k=1}^{N}\left(\frac{1}{6}\sum_{c=1}^{6}\left|\varepsilon_{c,k} - \varepsilon_{\text{nom } c,k}\right| - \text{MAER}\right)^2} \qquad \text{(Eq. 2)}$$

where "ε" represents the DVC-estimated strain; "ε_{nom}" represents the nominal virtually imposed strain; "c" represents the six independent strain components; "k" represents the measurement node; N is the number of nodes.

Lastly, in order to evaluate potential localizations of errors in the border due to the global deformable registration approach, the metrics were calculated after the removal of the most external layers of nodes perpendicular to the deformation direction. The same number of layers of nodes was removed from both sides of the image. This last analysis was performed for 1% of deformation along X, Y and Z for every specimen.

3 RESULTS

A total of 132 analyses were performed (four specimens, three loading directions, three load levels and nine regions of analysis for three loading direction of 1% of nominal deformation). The systematic and random errors are reported as median and standard deviation, among the specimens, for each component of strain and each simulated loading condition (Figure 2). The systematic errors of the normal strain component along X were 714±210, 864±193 and 985±131 microstrain for 1%, 2% and 3% of nominal deformation along X, respectively. Systematic errors of 1064±273, 1126±171 and 1091±96 microstrain have been found in the normal strain component along Y for 1%, 2% and 3% of deformation along Y, respectively. Finally, along Z the systematic errors computed for the normal strain component along Z were 775±211, 1036±165 and

974±191 microstrain for 1%, 2% and 3% deformation, respectively. Lower median systematic errors were found for the components of the strains with nominal values of 0 for tests performed along each normal direction and for each deformation level (range: -160 to 147 microstrain). Similar trends but higher errors were found for the median random error along the imposed deformation direction, which ranged from 1412±175 microstrain (1% deformation along Z direction) to 3697±405 microstrain (3% deformation along Z direction). Percentage difference between the median random errors and the nominal applied deformation were in the order of 10%: 14-16% for 1% deformation, 12-14% for 2% deformation and 10-12% for 3% deformation. Lower median random errors where found for the strain components with nominal values of 0 (range: 325 to 964 microstrain). As expected similar values for minimum principal strain and for the component of strain along the compressive directions were found and low values of maximum principal strains were found (Supplementary material).

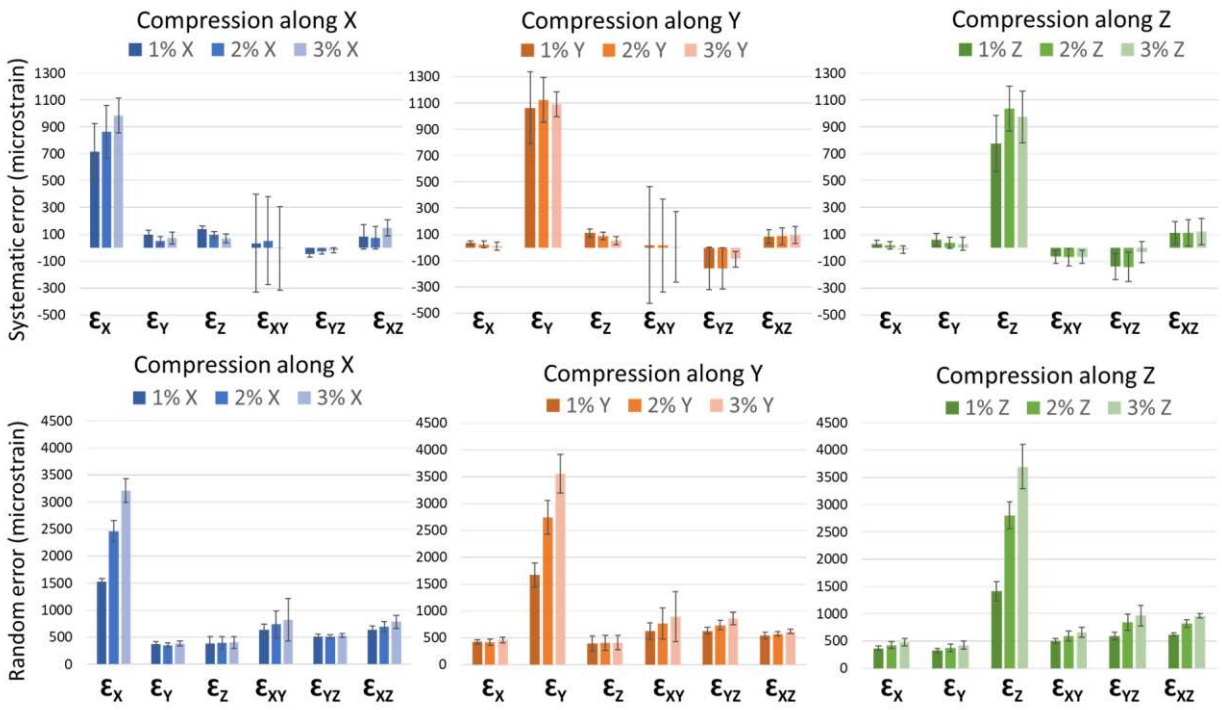

Figure 2. *Systematic (above) and random (below) errors for each component of strain, for each load level (1%, 2%, or 3%) and for each loading direction (X, Y, or Z). Bars and error bars represent the median and standard deviation among the specimens, respectively.*

The MAER ranged between 435 microstrain (1% deformation along Z direction) and 751 microstrain (3% deformation along Y direction) while the SDER ranged between 312 microstrain (1% deformation along Z

direction) and 684 microstrain (3% deformation along Y direction, Figure 3). As expected MAER and SDER tended to increase with the increasing of the applied deformation, for each direction (this trend was found for each specimen along each loading direction).

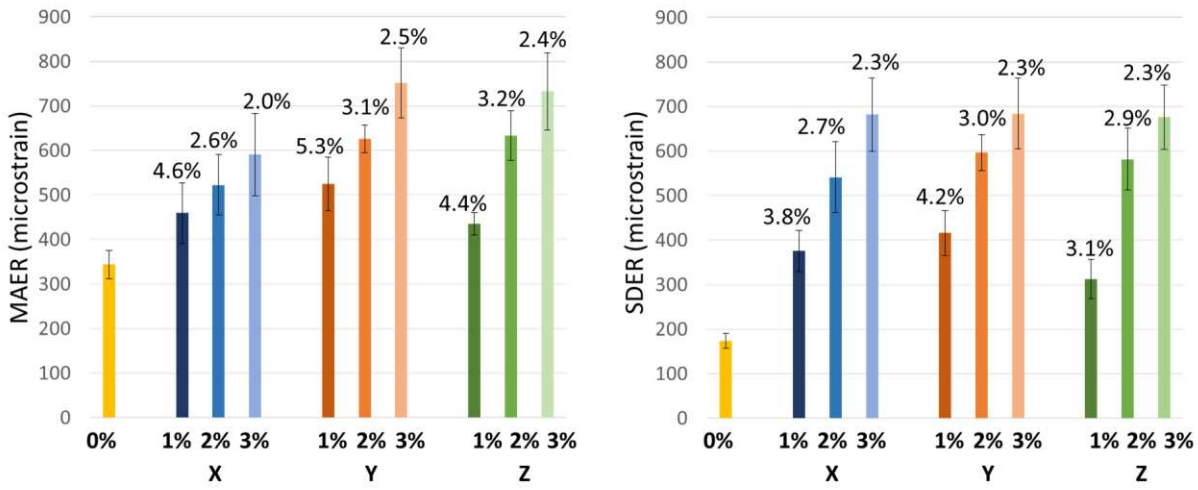

Figure 3. *Mean absolute error (MAER) and standard deviation of the error (SDER) for each load level (1, 2, or 3%) and each loading direction (X, Y, or Z). Bars and error bars represent the median and standard deviation among the specimens, respectively. Percentage values with respect to the applied deformation are reported above the bars. The values for the zero-strain condition (Palanca et al., 2017) are reported in yellow.*

All results reported above were found including in the analyses the entire volume of the deformed images. As reported in Table 1, the MEAR and SDER decreased when the layers of nodes closest to the border were removed. When 200 micrometers (12.5% of the nodes on both sides) were removed from the border, both MAER and SDER were comparable to the same errors in zero-strain condition, highlighting higher uncertainties of the DVC close to the border of the image. The systematic and random errors for the normal strain component along the deformation direction decreased when more layers of nodes were removed from the border along the loading direction (Figure 4 for loading along X), reaching a plateau at approximately 400 micrometer. The systematic and the random errors of the shear strain components remained almost constant with increasing number of the removed layers of nodes. Similar trends of the systematic and

random error have been found in all the loading directions (Supplementary material).

Table 1. *Median and standard deviation of MAER and SDER calculated among the specimens in function of the nominal deformation (along X, Y and Z) and the percentage of the total volume removed from the uncertainties analysis (5% to 45%, including both sides).*

		Volume removed								
		5%	*10%*	*15%*	*20%*	*25%*	*30%*	*35%*	*40%*	*45%*
MAER (microstrain)	**1% X**	459 ± 68	449 ± 69	425 ± 68	347 ± 57	336 ± 54	329 ± 52	325 ± 50	323 ± 49	321 ± 48
	1% Y	525 ± 60	454 ± 54	410 ± 48	384 ± 44	368 ± 41	357 ± 39	349 ± 38	344 ± 37	340 ± 37
	1% Z	435 ± 25	391 ± 22	367 ± 22	347 ± 22	333 ± 22	324 ± 22	321 ± 22	319 ± 23	318 ± 24
SDER (microstrain)	**1% X**	375 ± 46	265 ± 76	207 ± 102	151 ± 29	143 ± 23	141 ± 19	140 ± 16	140 ± 15	140 ± 15
	1% Y	416 ± 51	278 ± 43	210 ± 32	178 ± 26	159 ± 22	148 ± 20	146 ± 19	145 ± 19	145 ± 19
	1% Z	312 ± 44	220 ± 33	186 ± 25	173 ± 20	158 ± 18	148 ± 19	143 ± 21	140 ± 23	138 ± 25

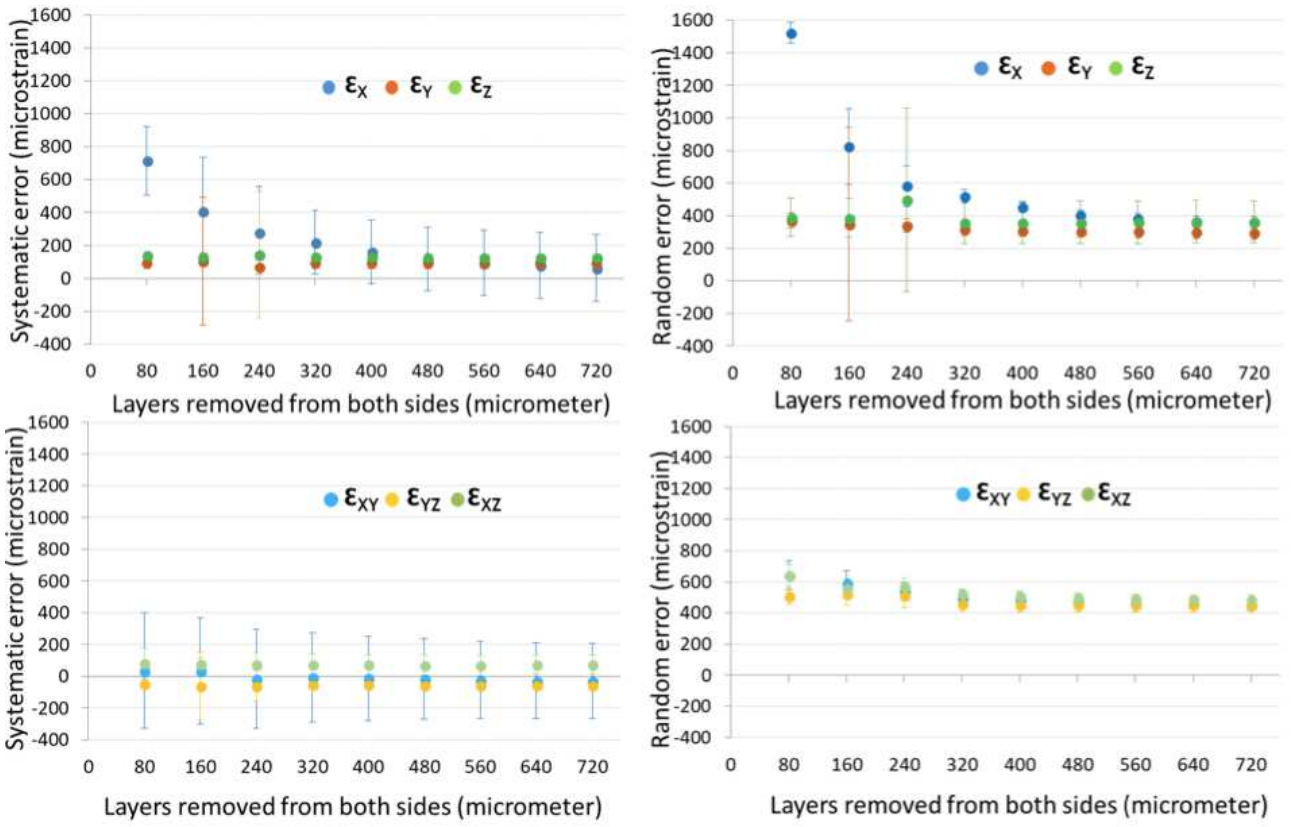

Figure 4. *Systematic (left) and random (right) errors of the normal and shear components of strain, for 1% of deformation along X, in function of the layers of nodes (reported as distance from the border along the loading direction) removed from the analyses. Markers and error bars represent the median and standard deviation among the specimens.*

The distribution of the strains along the different directions was in line with the virtually imposed deformation, with peaks of errors in the border of the image (example for one specimen virtually compressed up to 2% deformation is reported in Figure 5).

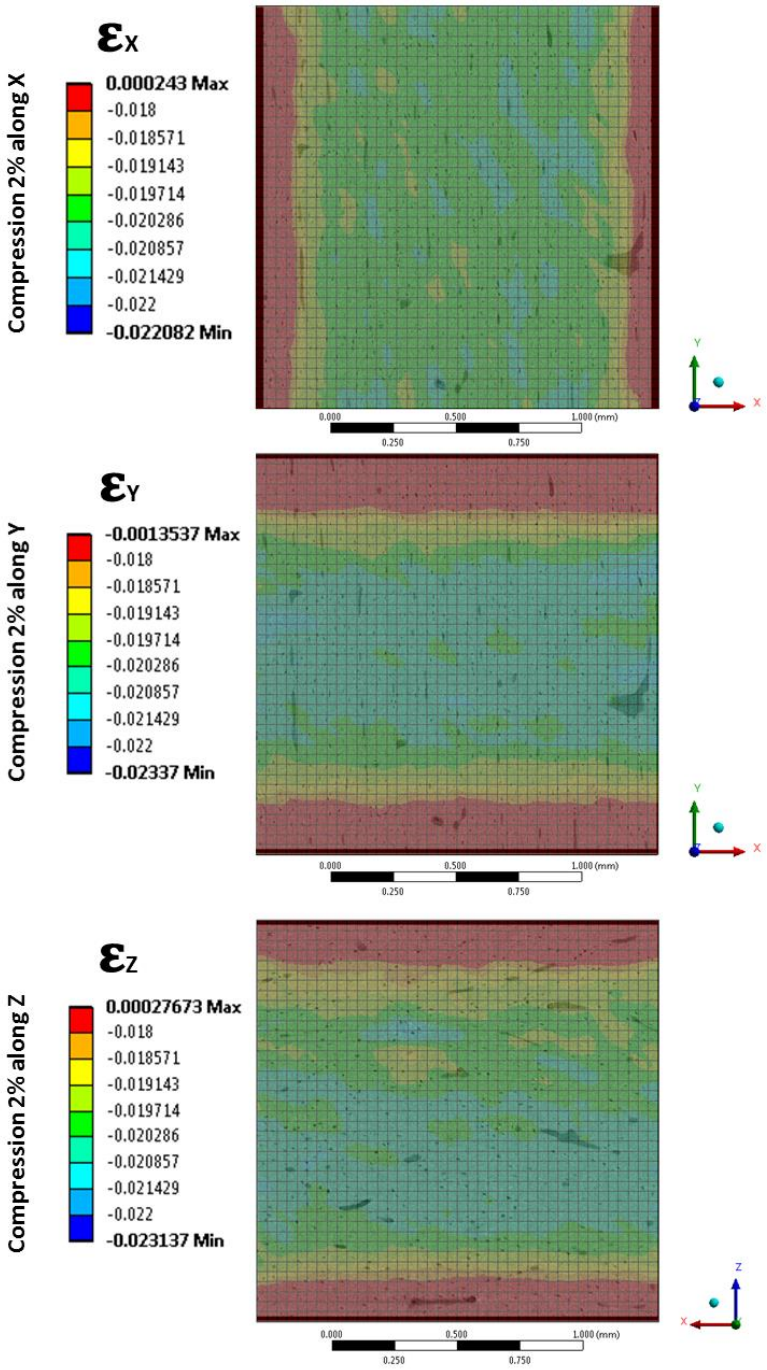

Figure 5: Spatial distribution of the normal strain components (ε_X, ε_Y and ε_Z) inside the Specimen 2, after virtual compression of 2%. In particular, the middle XY sections of the specimen for compression along X (top), along Y (center) and the middle XZ section of the specimen for compression along Z (bottom) are shown. The image of the corresponding section of the deformed image has been added in transparency.

4 DISCUSSION

The goal of this study was to evaluate the accuracy and precision of the BoneDVC approach under simulated deformation beyond the apparent bone yield strain.

The random error of the component of strain along the direction of the imposed deformation was larger when the deformation was larger, with percentage random error between 10% and 15% of the applied deformation. This trend may be due to the impact of the image noise on the DVC algorithm for higher level of deformation. It should be noted that in this study nominal deformations above the apparent yield strain for cortical bone (approximately 1%) (Bayraktar et al. 2004) have been considered, and more tests should be performed to evaluate the uncertainties of the method for small deformations.

Low variability in systematic and random errors for the different strain components have been found among specimens, except for one case (XY shear strain component for deformation along X or Y). This was due to a high error for one specimen. A possible explanation for this phenomenon could be differences in the morphologic structure of the pores (dimension and orientation) in that specimen. However, no significant correlations between the properties of the pores and the uncertainties have been found.

If the whole volume of the specimen is considered, higher values of SDER were found (2-4 times larger) compared to those obtained with zero-strain tests on the same images (Palanca et al. 2017). This different was mainly due to the higher errors in the normal strain component along the deformation direction, observed in this study. This result underlines that the most conservative way of analysing the uncertainties of the DVC method is with a repeated virtually deformed test, analyzing the outputs of each single strain component. Nevertheless, this work showed that the errors of the normal strain component, along the loading direction, were higher in the border of the VOI. While the localization of the errors could be due to algorithm artifacts close to regions without information in the image, this phenomenon did not involve only the first layer, but it propagates towards the center of the image for approximately 25% of the volume (400 micrometer). The errors in the middle of the specimen were similar to those obtained from zero-strain tests (SDER of approximately 150 microstrain), highlighting that this approach can be reasonable for most applications. The quantification of the error in the border for virtually deformed images may be different according to the used algorithm (global vs local) and the different bone microstructure (trabecular vs cortical bone). Finally, no prevalent direction of both systematic and random errors on the zero-strain components

has been observed, consistently with the literature (Tozzi et al. 2017; Palanca et al. 2015; Gillard et al. 2014).

The main limitations of this study were the low number of tested specimens with similar microstructure, the application of relatively simple virtual deformations (affine along one Cartesian direction) and the application of one type of DVC approach (global).

In conclusion a new method to evaluate the DVC strain measurements uncertainties has been presented and applied to SR-microCT images of cortical bone, adding insights in the application of such DVC algorithms for investigating anisotropic specimens. For the simulated deformation, uncertainties similar to those found in zero-strain test were found in the centre of the images, suggesting that this simpler approach can be used for similar deformation conditions (e.g. compression).

5 Acknowledgements

The authors would like to acknowledge Dr Chen, Dr Castro, Dr Campos-Marin, Dr Wittkowske, Dr Boldock, Dr Bodey and Dr Wanelik for help during the acquisition of the images at Diamond Light Source. We would like to acknowledge Prof Hose and Prof Barber for sharing the ShIRT library and Dr Fletcher and Dr Griffith for the implementation of the DVC service. We acknowledge Diamond Light Source for time at the Diamond-Manchester Imaging Beamline I13-2, under proposal MT10315. This study was partially funded by the FP7 European program MAMBO (PIEF-GA-2012-327357) and by the EPSRC Frontier Grant Multisim (EP/K03877X/1). Comini acknowledges the travel grant awarded by University of Bologna for research period abroad -E.F. 2017.

Declaration Statements

Conflict of interest

None declared

REFERENCES:

Barber, D. C., E. Oubel, A. F. Frangi, and D. R. Hose. 2007. “Efficient Computational Fluid Dynamics Mesh Generation by Image Registration.” *Medical Image Analysis* 11 (6): 648–62. https://doi.org/10.1016/j.media.2007.06.011.

Barber, D. C. and Hose, D. R. 2005. “Automatic segmentation of medical images using image registration: diagnostic and simulation applications.”, *Journal of medical engineering & technology*. doi: 10.1080/03091900412331289889.

Bay, B. K., Smith, T. S. , Fyhrie, D. P. , and Saad, M.. 1999. “Digital Volume Correlation: Three-Dimensional Strain Mapping Using x-Ray Tomography.” *Experimental Mechanics* 39 (3): 217–26. https://doi.org/10.1007/BF02323555.

Bayraktar, H. H., Morgan, E.F., Niebur, G.L., Morris, G.E., Wong, E.K., and Keaveny, T.. 2004. “Comparison of the Elastic and Yield Properties of Human Femoral Trabecular and Cortical Bone Tissue.” *Journal of Biomechanics* 37 (1): 27–35. https://doi.org/10.1016/S0021-9290(03)00257-4.

Chen, Y., Dall'Ara, E., Sales, E., Manda, K., Wallace, R., Pankaj, P., and Viceconti, M.. 2017. “Micro-CT Based Finite Element Models of Cancellous Bone Predict Accurately Displacement Once the Boundary Condition Is Well Replicated: A Validation Study.” *Journal of the Mechanical Behavior of Biomedical Materials* 65 (September 2015): 644–51. https://doi.org/10.1016/j.jmbbm.2016.09.014.

Christen, D., Levchuk, A., Schori, S., Schneider, P., Boyd, S.K., and Müller, R.. 2012. “Deformable Image Registration and 3D Strain Mapping for the Quantitative Assessment of Cortical Bone Microdamage.” *Journal of the Mechanical Behavior of Biomedical Materials* 8: 184–93. https://doi.org/10.1016/j.jmbbm.2011.12.009.

Costa, M. C., Tozzi, G., Cristofolini, L., Danesi, V., Viceconti, M., and Dall’Ara, E. 2017. “Micro Finite Element Models of the Vertebral Body: Validation of Local Displacement Predictions.” *PLoS ONE* 12 (7): 1–18. https://doi.org/10.1371/journal.pone.0180151.

Dall’Ara, E., Barber, D., and Viceconti, M.. 2014. “About the Inevitable Compromise between Spatial Resolution and Accuracy of Strain Measurement for Bone Tissue: A 3D Zero-Strain Study.” *Journal of Biomechanics* 47 (12): 2956–63. https://doi.org/10.1016/j.jbiomech.2014.07.019.

Dall’Ara, E., Peña-Fernández, M., Palanca,M., Giorgi,M., Cristofolini, L., and Tozzi, G.. 2017. “Precision of Digital Volume Correlation Approaches for Strain Analysis in Bone Imaged with Micro-Computed Tomography at Different Dimensional Levels.” *Frontiers in Materials* 4 (November). https://doi.org/10.3389/fmats.2017.00031.

Gillard, F., Boardman, R. , Mavrogordato, M. , Hollis, D. , Sinclair, I. , Pierron, F. , and Browne, M.. 2014. “The Application of Digital Volume Correlation (DVC) to Study the Microstructural Behaviour of Trabecular Bone during Compression.” *Journal of the Mechanical Behavior of Biomedical Materials* 29: 480–99. https://doi.org/10.1016/j.jmbbm.2013.09.014.

Grassi, L., and Isaksson, H. 2015. “Extracting Accurate Strain Measurements in Bone Mechanics: A Critical Review of Current Methods.” *Journal of the Mechanical Behavior of Biomedical Materials* 50: 43–54. https://doi.org/10.1016/j.jmbbm.2015.06.006.

Jackman, T. M., DelMonaco, A. M., & Morgan, E. F. 2016. “Accuracy of finite element analyses of CT scans in predictions of vertebral failure patterns under axial compression and anterior flexion. ” *Journal of Biomechanics*, *49*(2), 267–275. http://doi.org/10.1016/j.jbiomech.2015.12.004

Liu, L., and Morgan, E.F. 2007. “Accuracy and Precision of Digital Volume Correlation in Quantifying Displacements and Strains in Trabecular Bone.” *Journal of Biomechanics* 40 (15): 3516–20. https://doi.org/10.1016/j.jbiomech.2007.04.019.

Madi, K., Tozzi, G. , Zhang, Q. H. , Tong, J. , Cossey, A., Au, A. , Hollis, D. , and Hild, F. 2013. “Computation of Full-Field Displacements in a Scaffold Implant Using Digital Volume Correlation and Finite Element Analysis.” *Medical Engineering and Physics* 35 (9): 1298–1312. https://doi.org/10.1016/j.medengphy.2013.02.001.

Hardisty, M. R. and Whyne. C. M. 2009. “Whole Bone Strain Quantification by Image Registration: A Validation Study.” *J Biomech Eng* 131 (6): 064502

Oliviero, S., Giorgi, M., and Dall’Ara, E. 2018. “Validation of Finite Element Models of the Mouse Tibia Using Digital Volume Correlation.” *Journal of the Mechanical Behavior of Biomedical Materials* 86 (March): 172–84. https://doi.org/10.1016/J.JMBBM.2018.06.022.

Palanca, M., Bodey, A.J., Giorgi, M., Viceconti, M., Lacroix, D., Cristofolini, L., and Dall’Ara, E. 2017. “Local Displacement and Strain Uncertainties in Different Bone Types by Digital Volume Correlation of Synchrotron Microtomograms.” *Journal of Biomechanics* 58: 27–36. https://doi.org/10.1016/j.jbiomech.2017.04.007.

Palanca, M., Cristofolini, L., Dall’Ara, E., Curto, M., Innocente, F., Danesi, V., and Tozzi, G. 2016. “Digital Volume Correlation Can Be Used to Estimate Local Strains in Natural and Augmented Vertebrae: An Organ-Level Study.” *Journal of Biomechanics* 49 (16): 3882–90. https://doi.org/10.1016/j.jbiomech.2016.10.018.

Palanca, M., Tozzi, G., Cristofolini, L., Viceconti, M., and Dall'Ara, E. 2015. "Three-Dimensional Local Measurements of Bone Strain and Displacement: Comparison of Three Digital Volume Correlation Approaches." *Journal of Biomechanical Engineering* 137 (7): 071006. https://doi.org/10.1115/1.4030174.

Roberts, B.C., Perilli,E., and Reynolds, K.J.. 2014. "Application of the Digital Volume Correlation Technique for the Measurement of Displacement and Strain Fields in Bone: A Literature Review." *Journal of Biomechanics* 47 (5): 923–34. https://doi.org/10.1016/j.jbiomech.2014.01.001.

Sun Y., Pang, J.H., Wong, C.K., Su, F. 2005. "Finite Element Formulation for a Digital Image Correlation Method." *Appl Opt.* 44 (34): 7357–63.

Tozzi, G., Dall'Ara, E., Palanca, M., Curto, M., Innocente, F., and Cristofolini, L. 2017. "Strain Uncertainties from Two Digital Volume Correlation Approaches in Prophylactically Augmented Vertebrae: Local Analysis on Bone and Cement-Bone Microstructures." *Journal of the Mechanical Behavior of Biomedical Materials* 67 (November 2016): 117–26. https://doi.org/10.1016/j.jmbbm.2016.12.006.

Zauel, R. 2005. "Comparison of the Linear Finite Element Prediction of Deformation and Strain of Human Cancellous Bone to 3D Digital Volume Correlation Measurements." *Journal of Biomechanical Engineering* 128 (1): 1. https://doi.org/10.1115/1.2146001.

Zhu, M. L., Zhang, Q.H., Lupton, C., and Tong, J.. 2016. "Spatial Resolution and Measurement Uncertainty of Strains in Bone and Bone-Cement Interface Using Digital Volume Correlation." *Journal of the Mechanical Behavior of Biomedical Materials* 57 (April 2016): 269–79. https://doi.org/10.1016/j.jmbbm.2015.12.017.

Conflict of interest

Authors have no conflict of interest associated to this paper.

Supplementary material

Distribution of minimum and maximum principal strains

As expected the distributions of minimum principal strains for different loading directions and different loading values were very similar to those of the strain component along the loading direction (Fig. sup. 1). Moreover, the values of maximum principal strains were low and similar to the values of random errors found for the component of strains along the not-loaded directions (Fig. sup. 2).

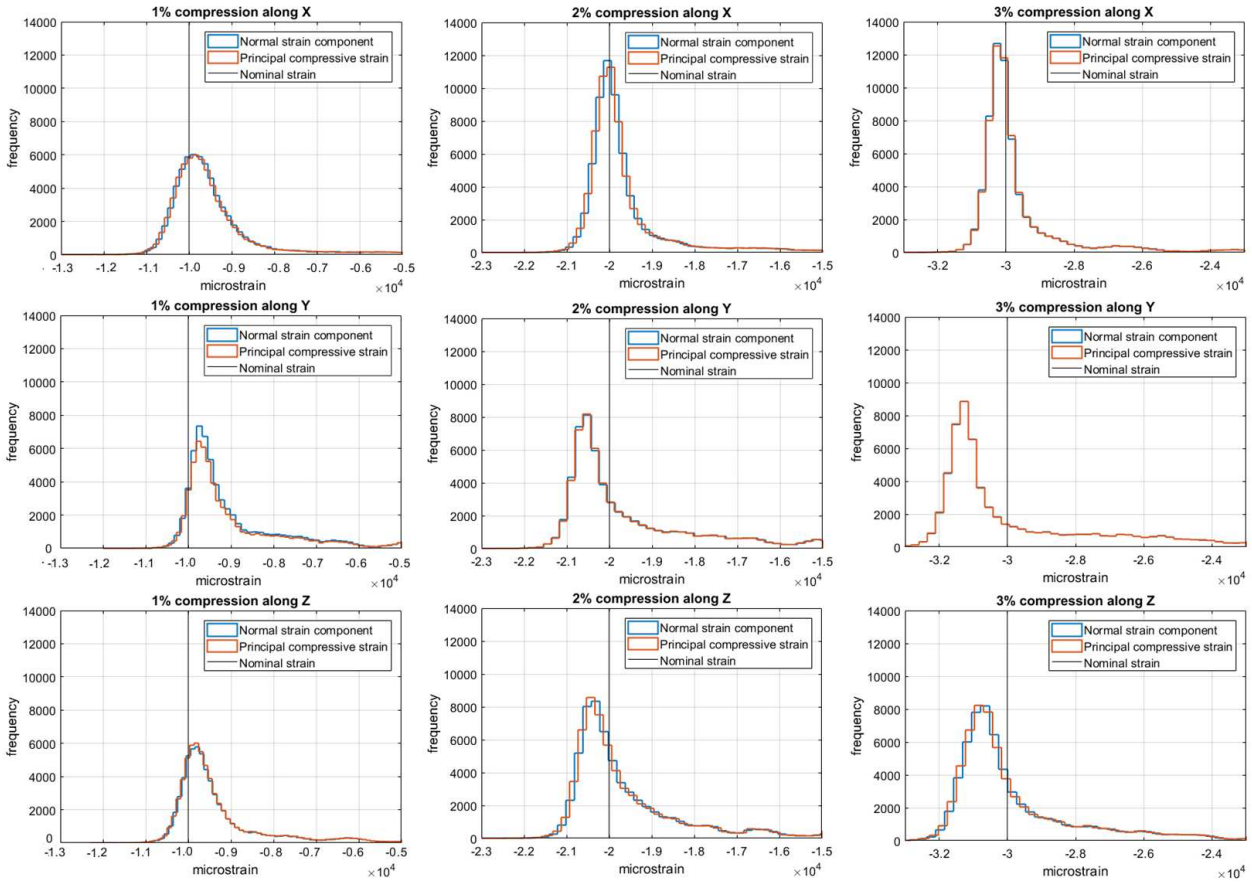

Fig. sup. 1. *Example of distributions of the values of the components of strain along the direction of loading (blue) and of the minimum (compressive) principal strain (red) for the different loading values (1%, 2% or 3%) along the different loading directions (X, Y or Z).*

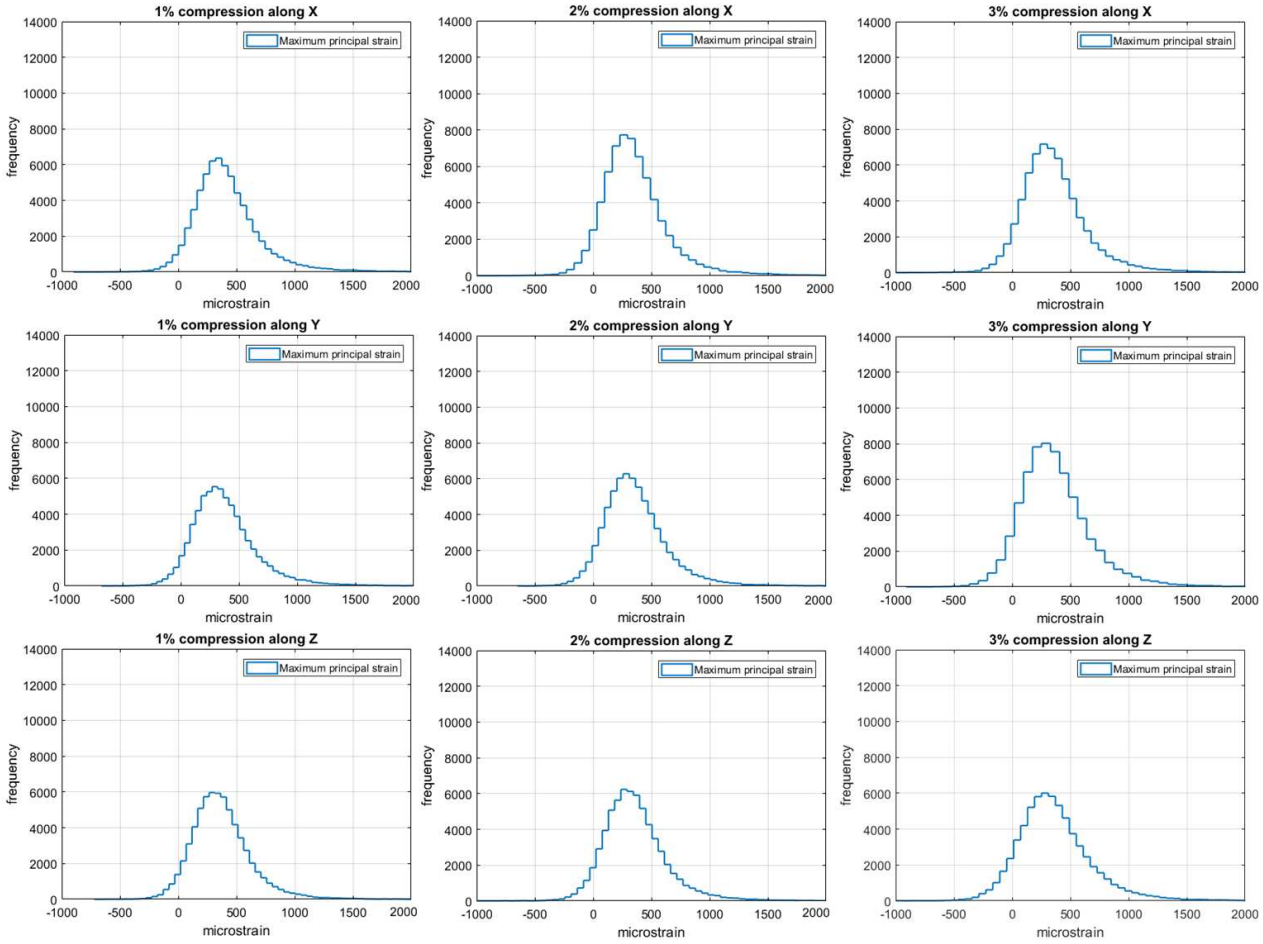

Fig. sup. 2. *Example of distributions of the values of the maximum principal strain (red) for the different loading values (1%, 2% or 3%) along the different loading directions (X, Y or Z).*

Error in function of number of layers of nodes removed from border

In order to evaluate potential border effects, various layers of nodes (of the computational grid) in the most external cells perpendicular to the deformation direction have been removed from the strain uncertainties analysis (Figure 4, Fig. sup. 3 and Fig. sup. 4). The layers have been removed symmetrically from both borders and have been expressed in physical dimension (micrometer). In all the direction tested (X in Figure 4, Y in Fig. Sup. 1 and Z in Fig. Sup. 2) for 1% of deformation, the systematic and random error of the normal strain component along the deformation direction showed a decreasing trend with increasing number layers of nodes were removed from the border. As expected, both systematic and random errors of the zero-strain components, for all directions of deformation, remained almost constant with increasing number of the removed layers. These results confirmed that the uncertainties were higher in the border of the VOI and they were consistent in all the directions of virtual deformation tested.

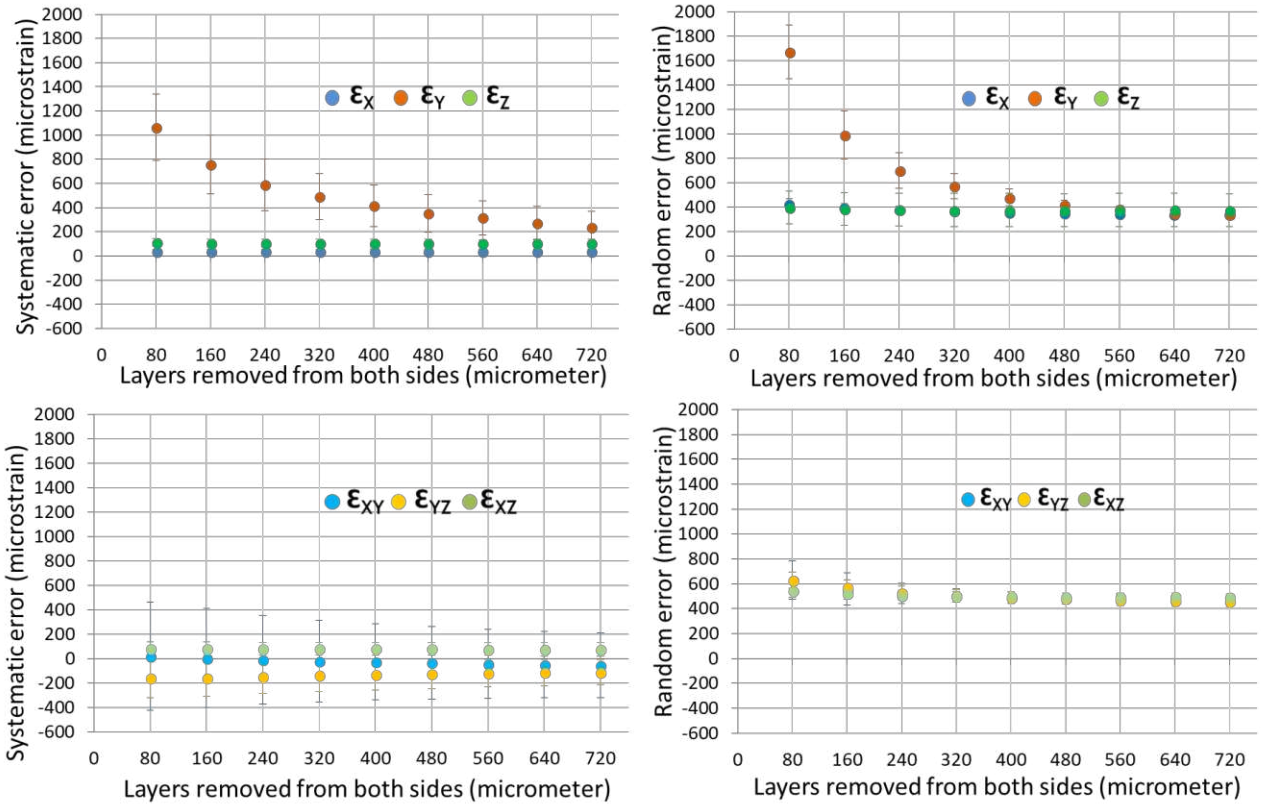

Fig. sup. 3. *Systematic (left) and random (right) errors of the normal and shear components of strain, for 1% of deformation along Y, in function of the layers of nodes (reported as distance from the border along the loading direction) removed from the analyses. Markers and error bars represent the median and standard deviation among the specimens.*

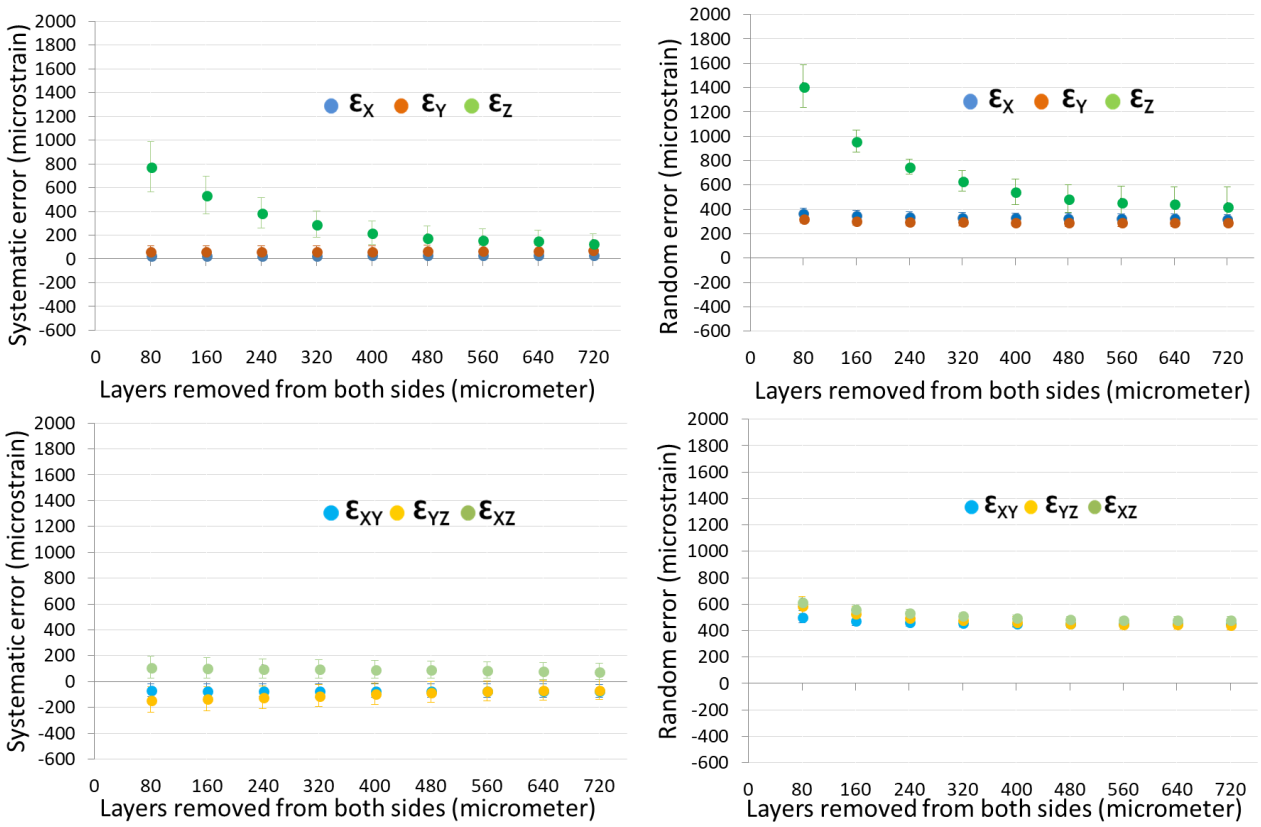

Fig. sup 4. *Systematic (left) and random (right) errors of the normal and shear components of strain, for 1% of deformation along Z, in function of the layers of nodes (reported as distance from the border along the loading direction) removed from the analyses. Markers and error bars represent the median and standard deviation among the specimens.*